IEEE Access
Multidisciplinary | Rapid Review | Open Access Journal

Received August 16, 2020, accepted August 27, 2020, date of publication September 2, 2020, date of current version September 15, 2020.

*Digital Object Identifier 10.1109/ACCESS.2020.3021083*

# Second-Order Linear Active Disturbance Rejection Control and Stability Analysis of Energy Storage Grid-Connected Inverter

**YOUJIE MA, LUYONG YANG, XUESONG ZHOU, AND XIA YANG**
Tianjin Key Laboratory for Control Theory and Applications in Complicated Industry Systems, School of Electrical and Electronic Engineering, Tianjin University of Technology, Tianjin 300384, China

Corresponding authors: Luyong Yang (183125317@stud.tjut.edu.cn) and Xuesong Zhou (zxsmyj@126.com)

This work was supported in part by the National Natural Science foundation of China under Grant 51877152, and in part by the Natural Science Foundation of Tianjin of China under Grant 18JCZDJC97300.

**ABSTRACT** At present, which has gradually become a technical development trend that the energy storage grid-connected inverter system is connected to the grid to ensure the stable operation of the whole system. However, the stability of the energy storage system itself is also very important for the safe operation of the power grid. Therefore, improving the stability of grid-connected energy storage system is still the key technology of current research. Aiming at the strong coupling and low-voltage ride-through fault of grid-connected system, a second-order mathematical model of grid-connected control system is established. Based on its state space model, a linear extended state observer (LESO) for state observation and a linear state error feedback (LSEF) control law for disturbance estimation are designed. The second-order linear active disturbance rejection control (LADRC) is introduced into the voltage loop, the stability of the second-order LADRC controller is proved by the Lyapunov stability theory, and the stability conditions are given. Finally, the simulation model of the grid-connected energy storage system is built on the MATLAB / Simulink digital platform, and the low-voltage ride-through fault is designed on the grid-side. The simulation results show that the effect of the second-order LADRC control is better than that of the traditional PI control obviously, which reflects the superiority of the second-order LADRC in controlling the grid-side low-voltage ride-through fault.

**INDEX TERMS** Energy storage grid-connected inverter system, linear active disturbance rejection control technology, linear extended state observer, Lyapunov stability theory, low-voltage ride-through.

## I. INTRODUCTION

In recent years, with the continuous development of new energy power generation technology, more stable and safe energy storage measures are of vital importance. At this stage, with the continuous connection of wind power generation systems and photo-voltaic power generation systems, the grid connection of energy storage systems has also become a hot-spot of current research [1]. For example, microgrid is a solution for managing additional power demand, which mainly generates electricity from renewable energy sources, such as renewable energy, solar, wind, and hydropower. Most renewable energies require energy storage systems because they are highly unpredictable in nature and require inverters to convert stored DC power into AC power to meet grid-connected requirements. Therefore, the realization of energy storage system access to the network is also a key technology developing currently [2]. Among them, the grid-connected inverter is a power electronic converter that realizes DC-AC conversion, and which is the core device connecting the system and the power grid [3]–[5]. Therefore, the control of the grid-connected inverter will directly affect the power quality of the grid-connected energy storage system and the ability of the system to operate safely and steadily. Besides, the grid-connected control applications of energy storage systems in other areas are also very extensive. For example, in order to further improve the grid-connected operation performance of wind turbines (WT) based on speed-regulated differential mechanism (SRDM). Reference [6] developed a hybrid power production device in which the hydrogen storage

The associate editor coordinating the review of this manuscript and approving it for publication was Qiu Ye Sun.

system (HSS) includes an electrolytic cell, hydrogen fuel cell and super capacitor are integrated into SRDM based on WT. After determining eight different working modes, a power monitoring method is proposed for the SRDM based on WT with HSS, which can realize the power flow management between energy and storage elements. The case study was conducted in the presence of different randomly varying wind speeds and grid voltage failures. The excellent performance of the wind-hydrogen hybrid system is well verified from the aspects of restraining the output power fluctuation and improving the continuous operation stability of the system. Reference [7] is based on a voltage source converter, taking into account unbalanced and non-linear working conditions, the battery energy storage system (BESS) is connected to the DC link of the VSC through a bidirectional DC-DC converter, which is a distributed generation (DG) unit control structure. This control structure is suitable for island operation and grid-connected operation mode of microgrid.

At present, the control of grid-connected mostly adopts the voltage and current double loop control of proportional integral (PI) regulator, which has the advantages of simple control structure and easy implementation, but which has great limitations on some occasions such as strong coupling, easy parameter perturbation, high-precision control and so on, so that in the actual working conditions, the traditional PI control is also difficult to achieve ideal control effect. Therefore, researcher Han Jingqing of Chinese Academy of Sciences proposed the concept of active disturbance rejection control (ADRC) technology on the basis of nonlinear PID controller [8], which only needs the rough model of the controlled object and the input and output signals of the system, then an extended state observer (ESO) can be designed to observe the total disturbance and unmodeled error of the system, and make feed-forward compensation in the control variables [9]. At present, the application of this control technology has been very extensive, not only that, but also the in-depth research on its control principle has also made great progress. For example, in the aspect of disturbance observer, reference [10] proposed a disturbance observer (DOB) for a class of nonlinear systems described by input-output differential equations observer design method, and has been applied successfully to nonlinear system disturbance estimation. In reference [11], an estimation method of induction motor speed regulation based on active disturbance rejection observer (ADRO) is proposed to realize sensorless control of induction motor, and external interference can be estimated immediately.

ADRC is a kind of nonlinear control technology, and which core is ESO [12]. When the state variables of the system are observed by ESO, the total disturbance of the system is observed, and the generalized state error is obtained, and the disturbance term is compensated and offset, so as to improve the stability and robustness of the control system. However, the traditional nonlinear ADRC contains too many parameters, so that it is difficult to set. Most of the research on this method in the design of control system is still in the simulation stage or get the similar optimal control effect by empirical method, and there is no perfect theoretical basis. In practical engineering application, although the nonlinear ADRC technology greatly improves the control performance of the system, but which increases the difficulty of controller design and parameter adjustment obviously. In reference [13], in order to reduce the number of parameter tuning, Professor Gao Zhiqiang, a famous American scholar, has carried out the linearization design of various structures of ADRC and proposed a linear active disturbance rejection control (LADRC) method. In this method, the concept of bandwidth is introduced into ADRC, and the parameters of ADRC are simplified into controller bandwidth and observer bandwidth by pole assignment method [14], and then the disturbance immunity and stability of LADRC are analyzed by frequency domain method [15]. The algorithm is simple and easy to implement in engineering, which reduces the difficulty of debugging greatly. Reference [16] starts with the frequency domain characteristics and analyzes the dynamic tracking estimation capability and filtering characteristics of the linear extended state observer (LESO). On this basis, the LADRC closed-loop transfer function and frequency band characteristic curve are obtained.Then, the system analyzes the stability of the controller, the dynamic suppression capability of external disturbances, the uncertainty of the control input gain, etc., and discusses the relationship between the above dynamic characteristics and parameter configuration. The LADRC reduces the control parameters to 3, and all have clear physical meanings, which is very convenient for engineering applications and has achieved good actual control effects. Reference [17] conducted in-depth discussions on the LADRC design of the missile flight control system, and conducted simulation studies, but did not conduct stability analysis. In reference [18], a first-order mathematical model of shunt hybrid active power filter for medium and high voltage system is established, and the stability of shunt hybrid active power filter with first-order LADRC controller is analyzed by Lyapunov stability theory. Considering that the grid-connected inverter in this paper is a second-order mathematical model, the second-order LADRC is used to control the grid-connected inverter with energy storage, and the Lyapunov stability of the second-order LADRC is analyzed.

This paper takes the control of grid-connected inverter as the research object, and takes the control of DC bus voltage as the research goal. Firstly, the mathematical model of grid-connected inverter in *dq*-axis rotating coordinate system is established, and the influence of power imbalance caused by grid-side low-voltage ride-through fault on DC bus voltage is analyzed [19]–[21]. Secondly, the second-order LADRC voltage outer loop controller is designed to form a new double closed-loop control strategy, and the linear state error feedback (LSEF) control law is designed. The final control variable is composed of the generated control variables and disturbance compensation quantities. Then, the stability of the second-order LADRC controller is analyzed through the Lyapunov stability theory, and which is

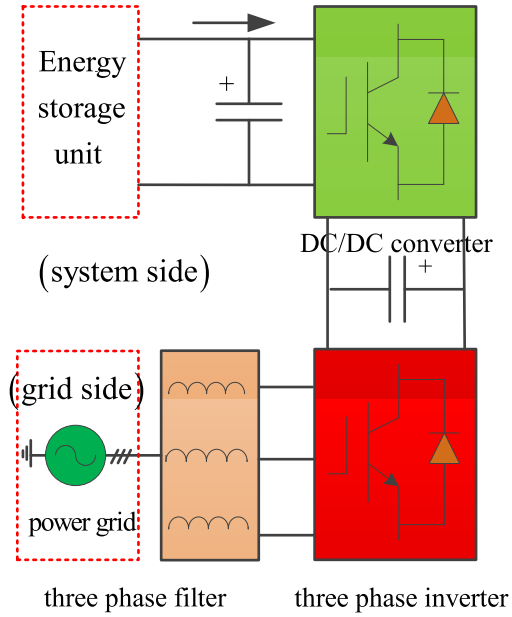


**FIGURE 1.** The two-stage grid-connected structure of the energy storage system.

proved that the second-order LADRC is stable progressively. Finally, through MATLAB & Simulink digital simulation, the superiority of the second-order LADRC controller under low-voltage ride-through fault on the grid-side is verified.

## II. MATHEMATICAL MODELING AND ENERGY ANALYSIS OF GRID-CONNECTED INVERTER

### A. ENERGY STORAGE CONVERSION SYSTEM

The two-stage grid-connected structure of the energy storage system is shown in Figure. 1.

It is composed of energy storage unit, power decoupling capacitor, DC/DC converter, three-phase inverter, three-phase filter and power grid. The DC/DC converter on the system side usually uses a Boost boost circuit to convert the lower DC voltage output on the energy storage unit side into a stable and higher DC voltage, which can meet the voltage amplitude of the grid-side inverter to the DC side value requirements. The grid-connected DC/AC converter mainly controls the grid-connected power factor and improves the grid-connected power quality.

Through the abstract, introduction and the control objectives of this article, we can know that the research direction of this article is the energy storage system, the controlled object is the grid-side grid-connected inverter, and the control objective is the DC side bus voltage. Therefore, the main research idea of this paper is to use the energy storage system to adopt a high-performance second-order LADRC strategy to analyze the stability of Lyapulov and to control the grid-connected inverter for better realization the stability of DC bus voltage.

### B. MATHEMATICAL MODELING OF GRID-CONNECTED INVERTER

The grid-side inverter control structure is shown in Figure 2 [22], [23]. Where $u_{dc}$ is the DC-side bus voltage, $i_{dc}$ is the

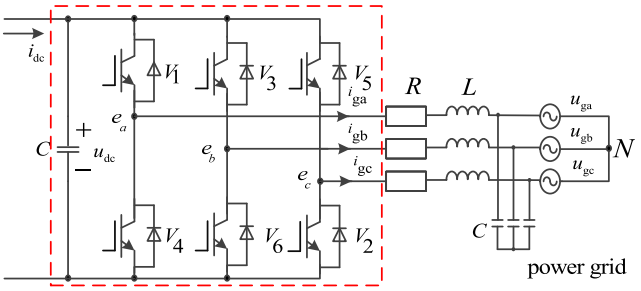


**FIGURE 2.** Overall control structure of grid-side inverter.

DC-side bus current, R, L, and C are the filter inductor internal resistance, filter inductance, and filter capacitor. Where $u_{ga}, u_{gb}, u_{gc}$ are represent the three-phase grid voltage respectively, and the $i_{ga}$, $i_{gb}$, $i_{gc}$ are represent the network current respectively.

According to Figure 1, the mathematical model of the grid-side inverter in the $dq$ rotating coordinate system [24] can be obtained:

$$\begin{cases} \dfrac{di_{\mathrm{gd}}}{dt} = \dfrac{1}{L}u_{\mathrm{gd}} + \omega i_{\mathrm{gq}} - \dfrac{R}{L}i_{\mathrm{gd}} - \dfrac{1}{L}e_{\mathrm{gd}} \\ \dfrac{di_{\mathrm{gq}}}{dt} = \dfrac{1}{L}u_{\mathrm{gq}} - \omega i_{\mathrm{gd}} - \dfrac{R}{L}i_{\mathrm{gq}} - \dfrac{1}{L}e_{\mathrm{gq}} \\ \dfrac{du_{\mathrm{dc}}}{dt} = i_{\mathrm{dc}} - \dfrac{3}{2C}\sum\limits_{k=d,q} S_{gk}i_{gk} \end{cases} \tag{1}$$

In equation (1), $e_{\mathrm{gd}}$, $e_{\mathrm{gq}}$ are the components of the grid voltage on the $dq$ axis, $u_{\mathrm{gd}}$, $u_{\mathrm{gq}}$ are the components of the grid-side inverter output voltage on the $dq$ axis, $i_{\mathrm{gd}}$, $i_{\mathrm{gq}}$ are the grid-side currents on the $dq$ axis component, $\omega$ is the fundamental frequency of the system, and $S_{gk}$ is the component of the system switching function on the $dq$ axis.

Simplifying the equation (1) will be obtained:

$$\frac{d^2u_{\mathrm{dc}}}{dt^2} = \frac{3}{2LC}\sum_{k=d,q} S_{\mathrm{gk}}\left(e_{gk} + i_{gk}R - u_{gk}\right) - \frac{\omega}{2C}\left(S_{\mathrm{gd}}i_{\mathrm{gq}} - S_{\mathrm{gq}}i_{\mathrm{gd}}\right) \tag{2}$$

It can be seen from equation (2) that under the $dq$ axis of the rotating coordinate system, the grid-connected inverter is a complex system with multiple variables and strong coupling, in the case of high accuracy requirements, which is difficult to meet the actual control requirements by using the traditional control method to control the DC bus voltage. Therefore, to achieve ideal control effect, the second-order LADRC with more representative and practical value is used in this paper.

### C. ENERGY ANALYSIS OF GRID-CONNECTED SYSTEM

The influence of power imbalance on DC bus voltage caused by grid-side low-voltage ride-through is analyzed from the energy point of view [25].

According to Figure. 3, the active power $P_{\mathrm{s}}$ output from the system side is input into the DC bus after passing through DC / DC, and the system output power $P_{\mathrm{s}}$ is equal to the grid-connected input power $P_{\mathrm{g}}$, which can be expressed by

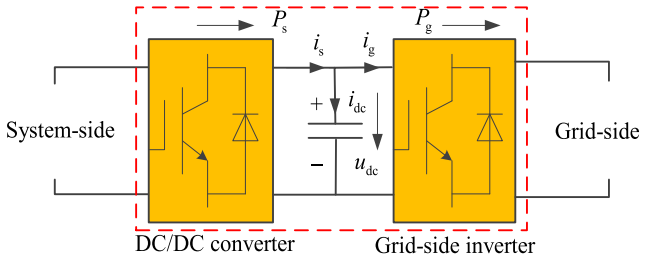


**FIGURE 3.** Schematic diagram of energy storage system.

the following equation:

$$P_s = u_{dc} i_s \tag{3}$$

In equation (3), where $i_s$ is the current output by the system-side inverter. The current $i_c$ flowing through the DC bus is:

$$i_c = c\frac{du_{dc}}{dt} = i_s - i_g \tag{4}$$

Excluding the losses of grid-connected inverter and AC side reactor:

$$P_g = u_{gd} i_d + u_{gq} i_q = u_{dc} i_q \tag{5}$$

When the grid voltage is stable, the power on both sides of the grid-connected inverter remains balanced. From the equation (3), (4) and (5) can get as:

$$cu_{dc}\frac{du_{dc}}{dt} = u_{dc} i_s - u_{dc} i_g = P_s - P_g = \Delta p \tag{6}$$

According to the theory of circuit theory, the energy stored in the capacitor $c$ on the DC side is:

$$cu_{dc}\frac{du_{dc}}{dt}\Delta T = \left(P_s - P_g\right)\cdot \Delta T = \Delta P \cdot \Delta T \tag{7}$$

From equation(7), we can see that when the grid voltage is not disturbed, the DC voltage $u_{dc}$ remains unchanged, and the $\Delta P$ value is zero. When the grid voltage drops, which $i_d$, $i_q$ remain unchanged, and the grid-connected output power $P_g$ will decrease inevitably. At this time, it can be considered that the energy supply on the energy storage system side is fixed during the voltage drop, which is equivalent to the active power $P_s$ emitted by the system side unchanged, $\Delta P$ will be greater than zero, resulting in unbalanced power across the inverter. Therefore, it is important to design a controller with excellent performance to ensure the stability of the DC-side bus voltage for the safety of the entire system.

## III. DESIGN OF SECOND-ORDER LADRC

### A. DESIGN OF THIRD-ORDER LESO

By adding the expansion state, the differential equation in equation (2) can be written as the state space form shown in equation (8).

$$\begin{cases} \begin{bmatrix} \dot{x}_1 \\ \dot{x}_2 \\ \dot{x}_3 \end{bmatrix} = \begin{bmatrix} 0 & 1 & 0 \\ 0 & 0 & 1 \\ 0 & 0 & 0 \end{bmatrix} \begin{bmatrix} x_1 \\ x_2 \\ x_3 \end{bmatrix} + \begin{bmatrix} 0 & 0 \\ b_0 & 0 \\ 0 & 1 \end{bmatrix} \begin{bmatrix} u \\ h \end{bmatrix} \\ y = x_1 \end{cases} \tag{8}$$

In the equation(8), $b_0 = 3/(2LC)$, where $x_1$, $x_2$ are the bus voltage and its differential, $x_3$ is the state variable expanded in LESO, that is, the total disturbance of the system, expressed as $f$, $h$ is used to represent the differential of $f$, the model of the total disturbance is as follows:

$$f = \frac{3}{2LC}\sum_{k=d,q} S_{gk}(i_{gk}R - u_{gk}) - \frac{\omega}{2C} \times \left(S_{gd} i_{gq} - S_{gq} i_{gd}\right) + \frac{3}{2LC} S_{gq} u_{gq} \tag{9}$$

According to equation (8), a third-order LESO can be established:

$$\begin{bmatrix} \dot{z}_1 \\ \dot{z}_2 \\ \dot{z}_3 \end{bmatrix} = \begin{bmatrix} -\beta_1 & 1 & 0 \\ -\beta_2 & 0 & 1 \\ -\beta_3 & 0 & 0 \end{bmatrix} \begin{bmatrix} z_1 \\ z_2 \\ z_3 \end{bmatrix} + \begin{bmatrix} 0 \\ b_0 \\ 0 \end{bmatrix} u + \begin{bmatrix} \beta_1 \\ \beta_2 \\ \beta_3 \end{bmatrix} y \tag{10}$$

In equation (10), $\beta_1$, $\beta_2$, $\beta_3$ are the coefficients of the observer.

### B. DESIGN OF LSEF CONTROL LAW

The control law of the system [26] is:

$$u = \frac{-z_3 + u_0}{b_0} \tag{11}$$

The PD control law can be designed as:

$$u_0 = k_p(v - z_1) - k_d z_2 \tag{12}$$

In equation (12), $k_p$ and $k_d$ are proportional and differential control gains. Choosing appropriate proportional differential gain coefficients can stabilize the system.

According to the pole configuration, the pole of equation (10) is arranged on the bandwidth $\omega_0$ of the observer, namely:

$$\begin{aligned} \lambda(s) &= s^3 + \beta_1 s^2 + \beta_2 s + \beta_3 \\ &= (s + \omega_0)^3 \end{aligned} \tag{13}$$

There are:

$$\begin{cases} \beta_1 = 3\omega_0 \\ \beta_2 = 3\omega_0^2 \\ \beta_3 = \omega_0^3 \end{cases} \tag{14}$$

Similarly, we can get:

$$\begin{cases} k_p = \omega_c^2 \\ k_d = 2\omega_c \end{cases} \tag{15}$$

Therefore, after parameterization, the parameters of the second-order LADRC can be simplified as the observer bandwidth $\omega_0$ and the controller bandwidth $\omega_c$, and the selection of $\omega_0$ and $\omega_c$ will affect the performance of LADRC directly.

According to the above analysis, the design of the second-order LADRC controller of the energy storage grid-connected system is shown in Figure 4:

### C. CONVERGENCE ANALYSIS OF THIRD-ORDER LESO

According to equations (10) and (14), the transfer functions of $Z_1$, $Z_2$, and $Z_3$ can be obtained:

$$\begin{cases} Z_1 = \dfrac{3\omega_0 s^2 + 3\omega_0^2 s + \omega_0^3}{(s+\omega_0)^3} y + \dfrac{b_0 s}{(s+\omega_0)^3} u \\ Z_2 = \dfrac{3\omega_0^2 s^2 + \omega_0^3 s}{(s+\omega_0)^3} y + \dfrac{b_0 (s+3\omega_0)\, s}{(s+\omega_0)^3} u \\ Z_3 = \dfrac{\omega_0^3 s^2}{(s+\omega_0)^3} y - \dfrac{b_0 \omega_0^3}{(s+\omega_0)^3} u \end{cases} \tag{16}$$

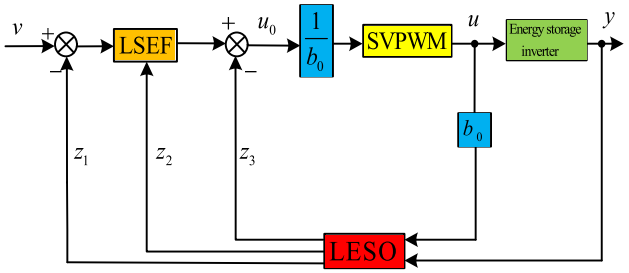


**FIGURE 4.** LADRC overall control structure.

Making the tracking errors $e_1 = z_1 - y$, $e_2 = z_2 - \dot{y}$, $e_3 = z_3 - f(y, \dot{y}, w)$ will be following as:

$$\begin{cases} e_1 = -\dfrac{s^3}{(s+\omega_0)^3} y + \dfrac{b_0 s}{(s+\omega_0)^3} u \\ e_2 = -\dfrac{(s+3\omega_0)\, s^3}{(s+\omega_0)^3} y + \dfrac{b_0 s}{(s+\omega_0)^3} u \\ e_3 = b_0 \left(1 - \dfrac{\omega_0^3}{(s+\omega_0)^3}\right) u - \left(1 - \dfrac{\omega_0^3}{(s+\omega_0)^3}\right) s^2 y \end{cases} \tag{17}$$

Considering the analysis typicality, $y$ and $u$ take the step signal $y(s) = K/s$, $u(s) = K/s$ whose amplitude is $K$, then the steady-state error can be obtained as:

$$\begin{cases} e_{1s} = \lim\limits_{s\to 0} s e_1 = 0 \\ e_{2s} = \lim\limits_{s\to 0} s e_2 = 0 \\ e_{3s} = \lim\limits_{s\to 0} s e_3 = 0 \end{cases} \tag{18}$$

The above equation shows that LESO has good convergence and estimation ability [27].

### D. ANTI-INTERFERENCE TRACKING ANALYSIS OF LADRC

First, according to equation (11), (12) and equation (15), we can get:

$$u = \frac{1}{b_0}\left(\omega_c^2 (v - z_1) - 2\omega_c z_2 - z_3\right) \tag{19}$$

Substituting equation (16) into equation (19) can get:

$$u = \frac{1}{b_0} G_1(s)\left[\omega_c^2 v - H(s)\, y\right] \tag{20}$$

In equation(20),

$$G_1(s) = \frac{(s+\omega_0)^3}{s^3 + 3\omega_0 s^2 + 3\omega_0^2 s + \omega_0^3 + \omega_c^2 s + 2\omega_c s^2 + 6\omega_0\omega_c s}$$

$$H(s) = \frac{\left(3\omega_0\omega_c^2 + 6\omega_c\omega_0^2 + \omega_0^3\right) s^2}{(s+\omega_0)^3} + \frac{\left(3\omega_0^2\omega_c^2 + 2\omega_c\omega_0^3\right) s + \omega_c\omega_0^3}{(s+\omega_0)^3}$$

According to equation (8), (11) and equation (12), the controlled object can be recorded as:

$$y = \frac{1}{s^2}(f + b_0 u) \tag{21}$$

Combining equation (20) and (21) can get:

$$y = \frac{\omega_c^2}{(s+\omega_c)^2} v + \frac{(s+\omega_c)^2 s + 3\omega_0 s (s + 2\omega_c + \omega_0)}{(s+\omega_0)^3 (s+\omega_c)^2} f \tag{22}$$

It can be seen from equation (22) that the output of the system consists of two parts: tracking term and disturbance term. When the disturbance term is ignored, the system can track quickly the reference input by adjusting the bandwidth $\omega_c$ of the controller, and the larger the value of $\omega_c$ is, the better the trace ability.

The disturbance term is caused by the dynamic observation error of LESO, and is an important factor affecting the control performance of the system. For this reason, the disturbance $f$ is taken as the unit step signal to analyze the immunity, then according to equation (22), the output response can be obtained as:

$$\begin{aligned} y(s) &= \frac{(s+\omega_c)^2 s + 3\omega_0 s (s + 2\omega_c + \omega_0)}{(s+\omega_0)^3 (s+\omega_c)^2} \frac{1}{s} \\ &= \frac{A_1}{(s+\omega_0)^3} + \frac{A_2}{(s+\omega_0)^2} + \frac{A_3}{s+\omega_0} \\ &\quad + \frac{B_1}{(s+\omega_c)^2} + \frac{B_2}{s+\omega_c} \end{aligned} \tag{23}$$

In equation (23):

$$A_1 = 1 + \frac{6\omega_0\omega_c}{(\omega_0 - \omega_c)^6}; \quad A_2 = \frac{3\omega_0^3 + 6\omega_0^2\omega_c - 9\omega_0\omega_c^2}{(\omega_0 - \omega_c)^4}$$

$$A_3 = \frac{6\omega_0^4 + 12\omega_0^3 + 9\omega_0^2\omega_c - 12\omega_0\omega_c^2}{2(\omega_0 - \omega_c)^5};$$

$$B_1 = \frac{3\omega_0(\omega_0 - \omega_c)}{(\omega_0 - \omega_c)^3}; \quad B_2 = \frac{-6\omega_0(\omega_0 - 2\omega_c)}{(\omega_0 - \omega_c)^4}$$

Laplace transform on it can get:

$$y(t) = \left(\frac{1}{2}A_1 t^2 + A_2 t + A_3\right) e^{-\omega_0 t} + (B_1 t + B_2)\, e^{-\omega_c t} \tag{24}$$

It can be seen that when time tends to infinity, the external disturbance output is 0 in the step state. Therefore, the second-order LADRC has good immunity to external disturbances.

### E. BASIC DESIGN PRINCIPLES OF LADRC PARAMETERS

The above analysis shows that LADRC parameters $\omega_0$ and $\omega_c$ have an important effect on the stability of the system, and the two can be adjusted independently. In addition, the choice of $b_0$ will also affect the dynamic characteristics of the system. According to the analysis of the above contents and the existing parameter design principles, the following parameter configuration methods are proposed in this section

1) For the controlled object whose model is known, convert its model to the corresponding form of state equation, and then calculate the approximate control gain $b_0$ in combination with the actual model equation. For the object that is difficult to establish a mathematical model, the ''time scale'' model identification method can be used to preliminarily select the control gain $b_0$ [28].

2) Selecting the initial values of parameters $\omega_c$ and $\omega_0$, keeping $\omega_c$ unchanged, and increasing $\omega_0$ gradually until the influence of noise is difficult to meet the system requirements.

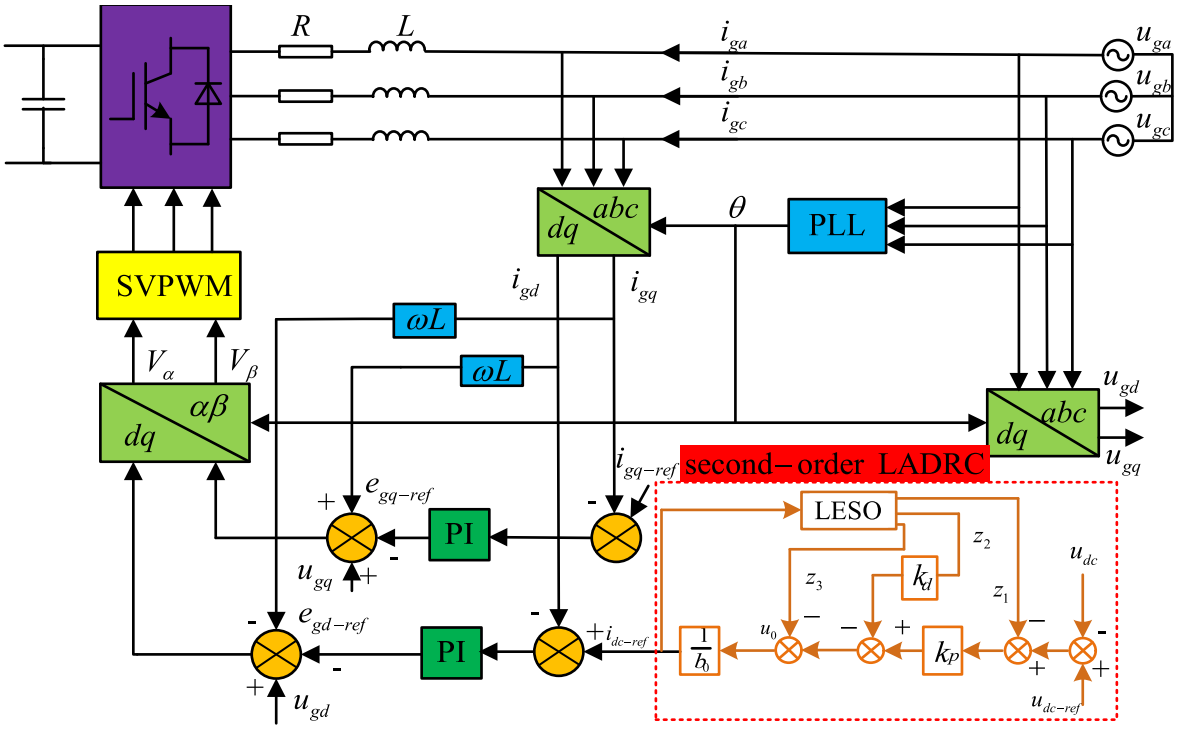


**FIGURE 5.** Control structure of grid-connected inverter combined with second-order LADRC.

3) Increasing $\omega_c$ gradually, decreasing $\omega_0$ when the impact of noise is unbearable and cause system output fluctuations, and then increase $\omega_c$ gradually, and adjust it in accordance with the cycle until it reaches the control requirements.

4) In the process of adjusting parameters, when the system dynamic tracking process has excessive oscillation, $b_0$ can be adjusted appropriately.

5) The second-order LADRC adopted in this paper selects $\omega_c = 3600$, $\omega_0 = 600$, $b_0 = 20000$ according to the above parameter design principles.

### *F. STRUCTURAL DESIGN OF GRID-CONNECTED INVERTER BASED ON LADRC*

It can be seen from equation (2) that the mathematical model [29], [30] of the grid-connected inverter is a second-order system, so the second-order LADRC is used for control. By analyzing the grid-connected inverter system, some known energy storage system model information can be integrated into the observer matrix, thereby improving the estimation accuracy effectively.

If the grid voltage is stable, in the $dq0$ coordinate system, the calculated reference current is compared with the actual current output by the grid to obtain the current deviation value [31]. After the PI regulator, the command voltage is obtained, and then the rotating coordinate system is transformed to the static coordinate system. Finally, the on-off of the switch tube is controlled by space vector pulse width modulation (SVPWM) to control the DC-side bus voltage [32], [22]. Therefore, the control structure of the grid-connected inverter combined with the second-order LADRC can be designed as Figure. 5.

## IV. STABILITY ANALYSIS OF SECOND-ORDER LADRC

It can be seen from Figure 3 that LADRC is a feedback system, and which essential problem is the stability of the system. This paper proves its stability for the second-order LADRC model [19], [19].

Taking the differential equation of the second-order system as an example for analysis:

$$\ddot{y} = -a_1\dot{y} - a_0 y + w + bu \tag{25}$$

In equation (25), where $u$ and $y$ are the input and output of the system, $w$ is the disturbance, $a_0$ and $a_1$ are the parameters of the system, $b$ is the input control gain, and $b_0$ is the estimated gain. Letting $x_1 = y$, $x_2 = \dot{y}$, defining $f(y, \dot{y}, w) = -a_1\dot{y} - a_0 y + w + (b - b_0)u$ as the system perturbation, letting $x_3 = f(y, \dot{y}, w)$, and assuming $\dot{f} = h$, the introduction of the expansion state $x_1, x_2, x_3$ to satisfy the following equation:

$$\begin{cases} \dot{x}_1 = x_2 \\ \dot{x}_2 = x_3 + b_0 u \\ \dot{x}_3 = h\left(\hat{X}, \omega\right) \\ y = x_1 \end{cases} \tag{26}$$

In equation (26), $X = [x_1\ x_2\ x_3]^{\mathrm{T}}$.

The third-order LESO of the continuous linear system corresponding to equation (26) can be designed as:

$$\begin{cases} \dot{z}_1 = z_2 + l_1\left(y - \hat{y}\right) \\ \dot{z}_2 = z_3 + l_2\left(y - \hat{y}\right) + b_0 u \\ \dot{z}_3 = l_3\left(y - \hat{y}\right) + h\left(\hat{X}, \omega\right) \\ \hat{y} = z_1 \end{cases} \tag{27}$$

In equation (27): $h\left(\hat{X},\omega\right)$ represents the unknown total disturbance observed by LESO.

Derived from the above equation, after parameterization, the poles of the characteristic equation can be placed at the same position $(-\omega_0, \omega_0)$, and the gain matrix of the observer is:

$$L = \begin{bmatrix} 3\omega_0 & 3\omega_0^2 & \omega_0^3 \end{bmatrix}^{\mathrm{T}} \tag{28}$$

Assuming $\tilde{y}_i = y_i - \hat{y}_i, i = 1, 2, 3$, the estimated error equation of LESO from equations (8) and (27) will be obtained:

$$\begin{cases} \dot{\tilde{y}}_1 = \tilde{y}_2 - 3\omega_0\tilde{y}_1 \\ \dot{\tilde{y}}_2 = \tilde{y}_3 - 3\omega_0^2\tilde{y}_1 \\ \dot{\tilde{y}}_3 = h\left(X,\omega\right) - h\left(\hat{X},\omega\right) - \omega_0^3\tilde{y}_1 \end{cases} \tag{29}$$

In equation (29): $h\left(X,\omega\right)$ represents the actual value observed by LESO. For further mathematical analysis of equation (29), we need to simplify the above equation, assuming $\varepsilon_j = \frac{\tilde{y}_j}{\omega_0^{j-1}}, j = 1, 2, 3$. Then the above equation (29) can be simplified to:

$$\begin{cases} \dot{\varepsilon}_1 = \omega_0\varepsilon_2 - 3\omega_0\varepsilon_1 \\ \dot{\varepsilon}_2 = \omega_0\varepsilon_3 - 3\omega_0\varepsilon_1 \\ \dot{\varepsilon}_3 = -\omega_0\varepsilon_1 + \dfrac{h\left(X,\omega\right) - h\left(\hat{X},\omega\right)}{\omega_0^2} \end{cases} \tag{30}$$

Further simplification can be obtained:

$$\dot{\varepsilon}_j = \omega_0 \begin{bmatrix} -3 & 1 & 0 \\ -3 & 0 & 1 \\ -1 & 0 & 0 \end{bmatrix} \begin{bmatrix} \varepsilon_1 \\ \varepsilon_2 \\ \varepsilon_3 \end{bmatrix} + \begin{bmatrix} 0 \\ 0 \\ 1 \end{bmatrix} \frac{h\left(X,\omega\right) - h\left(\hat{X},\omega\right)}{\omega_0^2} \tag{31}$$

In equation (31), let

$$A = \begin{bmatrix} -3 & 1 & 0 \\ -3 & 0 & 1 \\ -1 & 0 & 0 \end{bmatrix}, \quad B = \begin{bmatrix} 0 \\ 0 \\ 1 \end{bmatrix}, \quad \varepsilon = \begin{bmatrix} \varepsilon_1 \\ \varepsilon_2 \\ \varepsilon_3 \end{bmatrix}.$$

Knowing that the double pole of LESO is located at $\omega_0$, $A$ is Hurwitz stable, that is, there is a positive definite Hermitian matrix $P$ to satisfy $A$, then:

$$A^{\mathrm{T}}P + PA = -Q \tag{32}$$

And:

$$P = \begin{bmatrix} \frac{1}{16} & 0 & -\frac{3}{16} \\ 0 & \frac{3}{16} & -\frac{1}{2} \\ -\frac{3}{16} & -\frac{1}{2} & \frac{33}{16} \end{bmatrix}$$

In order to prove the stability of the controller, Lyapunov function is used for proof. The Lyapunov function is defined as follows [15]:

$$V\left(\varepsilon\right) = \varepsilon^{\mathrm{T}}P\varepsilon \tag{33}$$

There are:

$$\dot{V}\left(\varepsilon\right) = \varepsilon^{\mathrm{T}}P\dot{\varepsilon} + \dot{\varepsilon}^{\mathrm{T}}P\varepsilon \tag{34}$$

Combining equations (30) and (32), we can get:

$$\dot{V}\left(\varepsilon\right) = -\omega_0\varepsilon_3^2 + \frac{h\left(X,\omega\right) - h\left(\hat{X},\omega\right)}{\omega_0^2}\left(-\frac{3}{8}\varepsilon_1 - \varepsilon_2 + \frac{33}{8}\varepsilon_3\right) \tag{35}$$

Then there is the following theorem: Since $h\left(X,\omega\right)$ meets the Lipschitz continuity condition in the definition domain, then there is a constant $c$ that can satisfy the following expression:

$$\left|h\left(X,\omega\right) - h\left(\hat{X},\omega\right)\right| \le c\left\|X - \hat{X}\right\| \tag{36}$$

Then $\frac{h(X,\omega)-h\left(\hat{X},\omega\right)}{\omega_0^2}$ can satisfy the following equation:

$$\frac{h\left(X,\omega\right) - h\left(\hat{X},\omega\right)}{\omega_0^2}\left(-\frac{3}{8}\varepsilon_1 - \varepsilon_2 + \frac{33}{8}\varepsilon_3\right) \le c\left(-\frac{3}{8}\varepsilon_1 - \varepsilon_2 + \frac{33}{8}\varepsilon_3\right)\frac{\left\|X - \hat{X}\right\|}{\omega_0^2} \tag{37}$$

From equation (31) and equation (35), we can obtained:

$$-\frac{3}{8}\varepsilon_1 - \varepsilon_2 + \frac{33}{8}\varepsilon_3 = 2\varepsilon^{\mathrm{T}}PB \tag{38}$$

From equation (38), equation (37) can be further simplified to as follow:

$$2\varepsilon^{\mathrm{T}}PB\frac{h\left(X,\omega\right) - h\left(\hat{X},\omega\right)}{\omega_0^2} \le 2\varepsilon^{\mathrm{T}}PBc\frac{\left\|X - \hat{X}\right\|}{\omega_0^2} \tag{39}$$

When $\omega_0 \ge 1$, there is $\frac{\left\|X-\hat{X}\right\|}{\omega_0^2} = \frac{\left\|\tilde{X}\right\|}{\omega_0^2} \le \left\|\tilde{X}\right\|$, and because of the following expression (40):

$$\left\|PBc\right\|^2 - 2\left\|PBc\right\| + 1 \ge 0 \tag{40}$$

So available equation (41):

$$2\varepsilon^{\mathrm{T}}PB\frac{h\left(X,\omega\right) - h\left(\hat{X},\omega\right)}{\omega_0^2} \le \left(\left\|PBc\right\|^2 + 1\right)\left\|\varepsilon\right\|_1^2 \tag{41}$$

Simultaneous (38) and (41) are available:

$$\dot{V}\left(\varepsilon\right) \le -\omega_0\varepsilon_3^2 + \left(\left\|PBc\right\|^2 + 1\right)\left\|\varepsilon\right\|_1^2 \tag{42}$$

It can be seen from equation (38) that when $\omega_0 > \left\|PBc\right\|^2 + 1$, there are:

$$\dot{V}\left(\varepsilon\right) < 0 \tag{43}$$

According to the significance of Lyapunov's progressive stability, there are:

$$\lim_{t\to\infty}\tilde{y}_i\left(t\right) = 0, \quad i = 1, 2, 3 \tag{44}$$

Letting $e_i\left(t\right) = \tilde{y}_i\left(t\right)$, and from Lyapunov's asymptotic stability theorem, knowing that: assuming that $h\left(X,\omega\right)$

satisfies the global Lipschitz condition with respect to $X$, that is, there is a positive number $c$ that satisfies $\left|h(X,\omega)-h\left(\hat{X},\omega\right)\right| \leq c\left\|X-\hat{X}\right\|$ for any $\tilde{X}$, then there is a sufficiently large positive number $\omega$ such that $\lim_{t\to\infty} e_i(t)=0, i=1,2,3$. Combining the above derivation and combining equation (44), we can see that Lyapunov's asymptotic stability theorem holds, so the estimation error of the linearly expanded state observer is zero when the time tends to infinity, namely:

$$\lim_{t\to\infty} e_i(t)=0, \quad i=1,2,3 \tag{45}$$

According to equation (11) and equation (12):

$$u=\frac{k_{\mathrm{p}}(v-\hat{y}_1)-k_{\mathrm{d}}\hat{y}_2-\hat{y}_3}{b_0} \tag{46}$$

Makes $e=v-y_1$ can be obtained equation (47) from equation (46):

$$u=\frac{k_{\mathrm{p}}(\mathrm{e}+\tilde{y}_1)-k_{\mathrm{d}}(y_2-\tilde{y}_2)-(y_3-\tilde{y}_3)}{b_0} \tag{47}$$

$$\dot{e}=\dot{v}-\dot{y}=-k_{\mathrm{p}}(\mathrm{e}+\tilde{y}_1)-k_{\mathrm{d}}\tilde{y}_2+\tilde{y}_3+\dot{v} \tag{48}$$

To avoid the noise amplification effect of the linear tracking differentiator, which is not applied generally in LADRC, so equation (48) can be simplified as:

$$\dot{e}=\left[-k_{\mathrm{p}}\right]e(t)+\left[-k_{\mathrm{p}} \quad -k_{\mathrm{d}} \quad 1\right]\tilde{y}(t) \tag{49}$$

$-k_{\mathrm{p}}$ makes the characteristic polynomial $s-k_{\mathrm{p}}$ satisfy the Rolls criterion, so $\left[-k_{\mathrm{p}}\right]$ is Hurwitz stable and at the same time can be derived from equation (44): $\lim_{t\to\infty}\left\|\left[-k_{\mathrm{p}} \quad -k_{\mathrm{d}} \quad 1\right]\right\|\tilde{y}_i(t)=0$, so $\lim_{t\to\infty} e(t)=0$, according to the significance of Lyapunov's asymptotic stability, we know that LADRC is asymptotically stable, the stability of LADRC is proved and its stability condition is obtained.

## V. SIMULATION ANALYSIS

In order to verify the effectiveness of the control strategy designed in this paper, a simulation model of grid connection of energy storage system was built in MATLAB/Simulink [33], [34]. In this paper, the control of energy storage grid-connected inverter is taken as the research object, and the control of DC bus voltage is taken as the research goal. Where the PI control and the LADRC are compared and verified under grid voltage stability and fault respectively. Some parameters of the network side and controller of the energy storage system can refer to Appendix A and Appendix B.

### A. SIMULATION AND COMPARATIVE ANALYSIS OF VOLTAGE STABILITY OF GRID-CONNECTED ENERGY STORAGE SYSTEM

When the grid-side voltage is stable, that is, the grid-side voltage is not affected by internal and external interference, the grid-connected voltage waveform is shown in Figure 6(a). At this time, the DC bus voltage when the energy storage system is connected to the grid can be simulated and analyzed for the two different control methods of PI and LADRC. The DC side bus voltage is shown in Figure. 6 (b), and

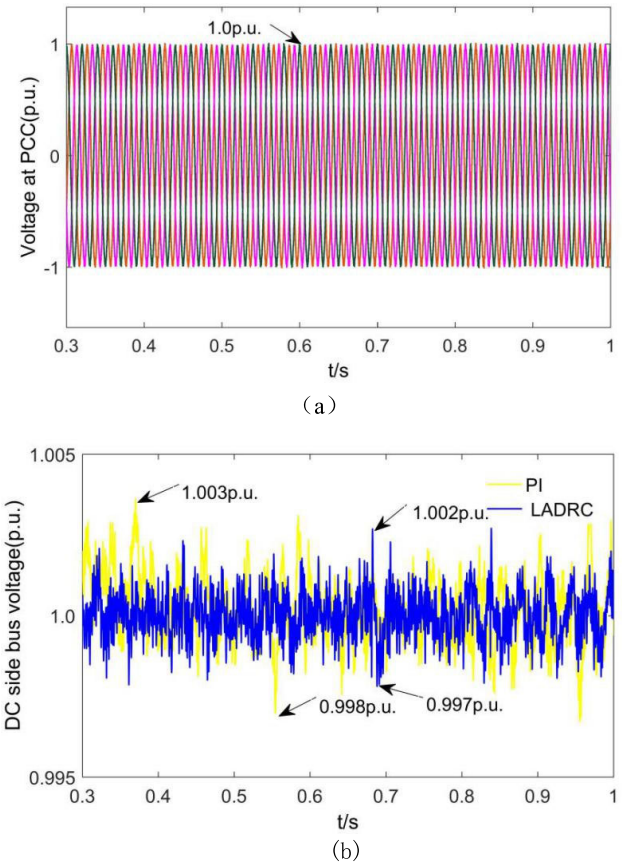


**FIGURE 6.** Comparative analysis of control effects under grid-side voltage stability. (a) Voltage waveform at grid connection point; (b) DC side bus voltage waveform.

the waveform analysis is carried out with anti-interference performance and dynamic response as the main performance indexes.

As can be seen from Figure 6(b), when the grid-side voltage is in a stable state, the DC bus voltage change range under PI control is 0.998p.u.-1.003p.u., and the DC side bus voltage change range under LADRC is 0.997p.u.-1.002p.u., which control effect is slightly better than PI control. However, in actual engineering applications, the optimization and improvement of the controller design are carried out through the situation of grid-side voltage failure. In general, in the state where the grid voltage is stable, the control effect of the controller is basically not very obvious, but it will be slightly better than the traditional control. Therefore, in the next simulation comparison experiment, the main design is the low-voltage ride-through fault on the grid-side as an unstable state to compare and analyze the control effect of the controller.

### B. COMPARATIVE ANALYSIS OF SIMULATIONS UNDER GRID-SIDE VOLTAGE FAULTS IN ENERGY STORAGE SYSTEMS

In practical engineering, the grid-connected energy storage system will be affected by grid-side voltage fluctuation. To further verify the effectiveness of LADRC voltage outer loop control effect and make the controller normal application in

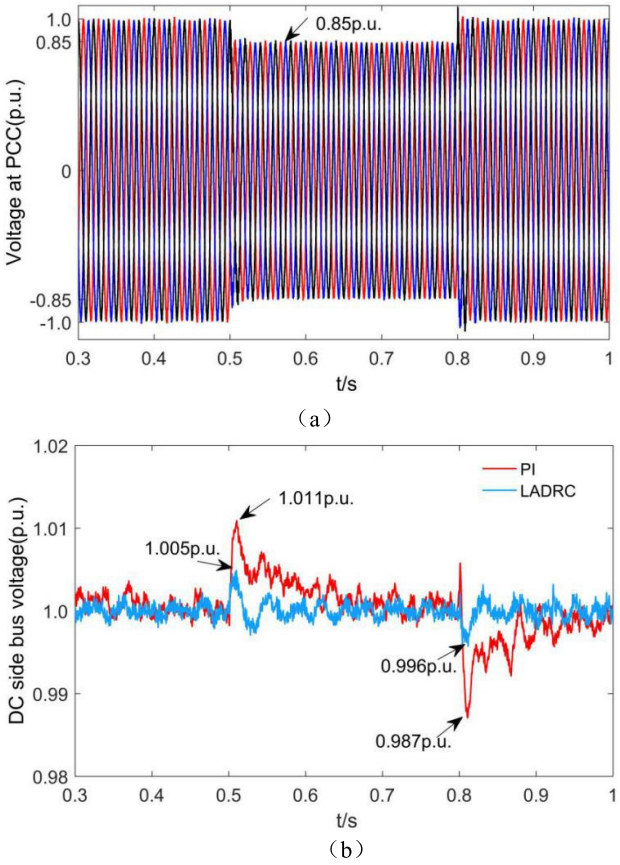


**FIGURE 7.** Comparative analysis of the control effect of grid-side low-voltage ride-through 15%. (a) Voltage waveform at grid connection point; (b) DC side bus voltage waveform.

the actual energy storage system, aiming at two different control modes of LADRC and PI, this paper designs the grid-side low-voltage ride-through fault [35]–[40] of energy storage system, so as to prove the effectiveness of the LADRC control.

### 1) SIMULATION AND COMPARATIVE ANALYSIS OF GRID-SIDE VOLTAGE SYMMETRICAL CROSSING 15%

Setting the grid-connected side voltage to drop symmetrically by 15% due to the fault. The fault starts at t = 0.5 s and ends at t = 0.8 s. The grid-connected voltage waveform is shown in Figure 7(a). The other conditions are the same. Compare the dynamic response waveform of the DC-side bus voltage under the grid-side voltage drop of 15% under the two control methods, as shown in Figure 7(b). Select the voltage fluctuation range and voltage stability as important reference indexes for control performance.

As can be seen from Figure 7(b), the bus voltage fluctuation range under PI control is 0.987p.u.-1.011p.u., while the DC bus voltage controlled by LADRC during the low-voltage ride-through 0.85p.u. fluctuates in the range 0.996p.u.-1.005p.u., and can reach the steady state 1.0p.u. quickly. In contrast, LADRC has a better promotion effect on the stability of the DC bus voltage under disturbance conditions, indicating that LADRC has better anti-interference performance.

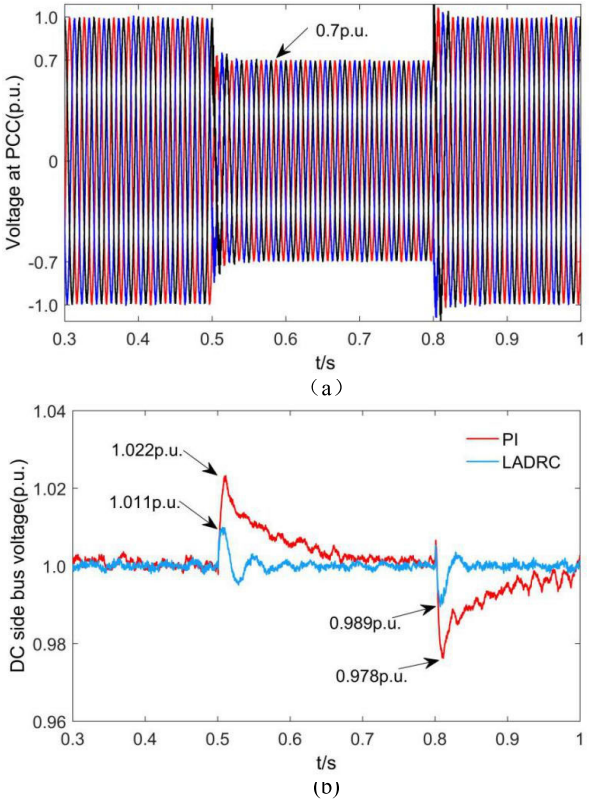


**FIGURE 8.** Comparative analysis of the control effect of grid side low voltage ride through 30%. (a) Voltage waveform at grid connection point; (b) DC side bus voltage waveform.

### 2) SIMULATION AND COMPARATIVE ANALYSIS OF GRID-SIDE VOLTAGE SYMMETRICAL CROSSING 30%

It is set that the grid-side voltage drops by 30% symmetrically due to fault, and the fault starts when t = 0.5 s, and ends when t = 0.8 s. the voltage waveform of the grid connection point is shown in Figure. 8(a). Other dynamic response waveform of DC side bus voltage dropping by 30% symmetrically at the grid-side are shown in Figure. 8 (b).

As can be seen from Figure 8(b), the bus voltage fluctuation range under PI control is 0.978p.u.-1.011p.u., while the DC bus voltage controlled by LADRC during the low-voltage ride-through 0.7p.u. fluctuates in the range 0.989p.u.-1.022p.u., and can reach the steady state 1.0p.u. quickly. In contrast, LADRC control has a better promotion effect on the stability of the DC bus voltage under disturbance conditions, indicating that the LADRC has better anti-interference performance. Compared with the symmetrical voltage drop of 0.85p.u. on the grid-side, the fluctuation range of the DC-side bus voltage is larger significantly. It can be seen that the symmetrical drop of the grid-side voltage affects the fluctuation range of the DC-side bus voltage. The greater the voltage drop, the larger the fluctuation range of the DC side bus voltage; the smaller the voltage drop, the smaller the fluctuation range of the DC side bus voltage. Therefore, the voltage outer loop controller to ensure the stability of the DC side bus voltage is crucial to the stable operation of the entire system.

**TABLE 1. Parameters of grid-connected side of storage system.**

| Symbol | Quantity | Value | Unit |
|---|---|---|---|
| $V_g$ | Rated voltage | V | 590 |
| $f$ | Rated Frequency | HZ | 50 |
| $u_{dc}$ | DC-side bus voltage | V | 1070 |
| $C$ | DC-side bus capacitor | $\mu$F | 240 |
| $R$ | Grid-side filter resistance | Ω | 0.942 |
| $C$ | Grid-side filter capacitor | $\mu$F | 147 |
| $L$ | Grid-side filter inductance | mH | 120 |

**TABLE 2. Controller parameters.**

| Symbol | Quantity | Value |
|---|---|---|
| $\omega_c$ | Controller bandwidth | 3600 |
| $\omega_0$ | Observer bandwidth | 600 |
| $b_0$ | Control gain | 20000 |

## VI. IN CONCLUSION

The DC link bus voltage control of the grid-connected inverter is an important issue in the stable grid connection of the energy storage system. This paper proposes a second-order LADRC strategy to optimize the grid-connected inverter system. The model design of the second-order LADRC can track the change of the command signal well, and deal with the contradiction between the speed and overshoot in the control process, and avoid the cumbersome decoupling control design, further simplifying the controller, reflecting the advantages of LADRC are met, and the demand for grid connection under the condition of grid voltage fluctuation is met. In addition, since the core concern of this paper is the stability of the energy storage grid-connected inverter system when it is connected to the grid, and the core of this focus is the application of the controller, so this paper introduces second-order LADRC in the voltage loop. The rigorous mathematical derivation through the Lyapunov stability theory proves the stability of the second-order LADRC, and gives the asymptotic stability conditions. Finally, for the simulation model of the energy storage system, a low-voltage ride-through fault is designed on the grid-side, and the simulation results of different kinds of working conditions also verify the correctness and feasibility of the theoretical analysis.

However, the design of this paper also has certain flaws, especially under the design of high-voltage ride-through conditions on the grid-side, the control effect of using second-order LADRC is not significantly superior to traditional PI control. Analyzing the reason, on the one hand, it may be due to the insufficient design of the controller, on the other hand, it may be due to the adjustment of parameters. Therefore, in view of the above deficiencies, I will conduct an in-depth analysis in the following topic research.

## APPENDIX A

## APPENDIX B

## REFERENCES


[1] Y. Li, D. W. Gao, W. Gao, H. Zhang, and J. Zhou, "Double-mode energy management for multi-energy system via distributed dynamic event-triggered Newton-raphson algorithm," *IEEE Trans. Smart Grid*, early access, Jun. 26, 2020, doi: 10.1109/TSG.2020.3005179.

[2] R. Islam, M. Hasan, F. R. Badal, S. K. Das, and S. K. Ghosh, "A Blended Improved H5 Topology With ILQG Controller to Augment the Performance of Microgrid System for Grid-Connected Operations," *IEEE Access*, vol. 8, pp. 69639–69660, 2020, doi: 10.1109/ACCESS.2020.2986213.

[3] M. H. Qais, H. M. Hasanien, and S. Alghuwainem, "A grey wolf optimizer for optimum parameters of multiple PI controllers of a grid-connected PMSG driven by variable speed wind turbine," *IEEE Access*, vol. 6, pp. 44120–44128, 2018.

[4] M. M. Rajan and S. A. Daniel, "MPPT with single DC–DC converter and inverter for grid-connected hybrid wind-driven PMSG–PV system," *IEEE Trans. Ind. Electron.* , vol. 62, no. 8, pp. 4849–4857, Aug. 2015.

[5] Z. Zhang, F. Wang, J. Wang, J. Rodríguez, and R. Kennel, "Nonlinear direct control for three-level NPC back-to-back converter PMSG wind turbine systems: Experimental assessment with FPGA," *IEEE Trans. Ind. Informat.*, vol. 13, no. 3, pp. 1172–1183, Jun. 2017.

[6] W. YIN, L. LIU, and A. X. RUI, "Analysis, modeling and control of a hybrid drive wind turbine with hydrogen energy storage system," *IEEE Access*, vol. 8, pp. 114795–114806, 2020, doi: 10.1109/ACCESS.2020.3003798.

[7] N. R. Merritt, C. Chakraborty, P. Bajpai, and B. C. Pal, "A unified control structure for grid connected and islanded mode of operation of voltage source converter based distributed generation units under unbalanced and non-linear conditions," *IEEE Trans. Power Del.*, vol. 35, no. 4, pp. 1758–1768, Aug. 2020.

[8] J. Han, "From PID to active disturbance rejection control," *IEEE Trans. Ind. Electron.*, vol. 56, no. 3, pp. 900–906, Mar. 2009.

[9] L. Yang, J. Zeng, W. Ma, and Z. Huang, "Voltage control of micro-grid inverter based on improved second order linear active disturbance rejection technology," *Power System. Autom*, vol. 43, pp. 685–703, 2019.

[10] S. H. Ding, W. H. Chen, K. Q. Mei, and J. David Murray-Smith, "Disturbance observer design for nonlinear systems represented by input–output models," *IEEE Trans. Ind. Electron.*, vol. 67, no. 2, pp. 1222–1232, Feb. 2020, doi: 10.1109/TIE.2019.2898585.

[11] C. Du, Z. Yin, J. Liu, Y. Zhang, and X. Sun, "A speed estimation method for induction motors based on active disturbance rejection observer," *IEEE Trans. Power Electron.*, vol. 35, no. 8, pp. 8429–8442, Aug. 2020, doi: 10.1109/TPEL.2020.2964573.

[12] D. Wu and K. Chen, "Frequency-domain analysis of nonlinear active disturbance rejection control via the describing function method," *IEEE Trans. Ind. Electron.*, vol. 60, no. 9, pp. 3906–3914, Sep. 2013.

[13] Z. Gao, Y. Huang, and J. Han, "An alternative paradigm for control system design," in *Proc. 40th IEEE Conf. Decis. Control*, Orlando, FL, USA, Dec. 2001, pp. 4–7.

[14] Z. Gao, "Scaling and bandwidth-parameterization based controller tuning," in *Proc. Amer. Control Conf.*, Denver, CO, USA, Jun. 2003, pp. 4989–4996.

[15] Z.-Q. Chen, M.-W. Sun, and R.-G. Yang, "On the stability of linear active disturbance rejection control," *Acta Automatica Sinica*, vol. 39, no. 5, pp. 574–580, Mar. 2014.

[16] D. Yuan, X. J. Ma, Q. Zeng, and X. Qiu, "Research on frequency-band characteristics and parameters configuration of linear active disturbance rejection control for second-order systems," *Control Theory Appl.*, vol. 30, no. 12, pp. 1630–1640, 2013.

[17] R. Yang, M. Sun, and Z. Chen, "Active disturbance rejection control on first-order plant," *J. Syst. Eng. Electron.*, vol. 22, no. 1, pp. 95–102, Feb. 2011.

[18] M. A. Youjie, Z. Jian, Z. Xuesong, and T. Chengwen, "A linear auto disturbance rejection controller for shunt hybrid active power filters and its stability analysis," *Power Syst. Technol.*, vol. 3, no. 11, pp. 211–216, 2012.

[19] J. Liu, W. Yao, J. Fang, J. Wen, and S. Cheng, "Stability analysis and energy storage-based solution of wind farm during low voltage ride through," *Int. J. Electr. Power Energy Syst.*, vol. 101, pp. 75–84, Oct. 2018.
[20] J. F. Conroy and R. Watson, "Low-voltage ride-through of a full converter wind turbine with permanent magnet generator," *IET Renew. Power Gener.*, vol. 1, no. 3, pp. 182–189, 2017.
[21] M. Nasiri, J. Milimonfared, and S. H. Fathi, "A review of low-voltage ride-through enhancement methods for permanent magnet synchronous generator based wind turbines," *Renew. Sustain. Energy Rev.*, vol. 4, pp. 399–415, Jul. 2015.
[22] J.-S. Lee, K.-B. Lee, and F. Blaabjerg, "Predictive control with discrete space-vector modulation of vienna rectifier for driving PMSG of wind turbine systems," *IEEE Trans. Power Electron.*, vol. 34, no. 12, pp. 12368–12383, Dec. 2019.
[23] W. Rui, S. Qiuye, M. Dazhong, and H. Xuguang, "Line impedance cooperative stability region identification method for grid-tied inverters under weak grids," *IEEE Trans. Smart Grid*, vol. 11, no. 4, pp. 2856–2866, Jul. 2020.
[24] Y. X. Su, C. H. Zheng, and B. Y. Duan, "Automatic disturbances rejection controller for precise motion control of permanent-magnet synchronous motors," *IEEE Trans. Ind. Electron.*, vol. 52, no. 3, pp. 814–823, Jun. 2005.
[25] Q. Sun, R. Han, H. Zhang, J. Zhou, and J. M. Guerrero, "A multiagent-based consensus algorithm for distributed coordinated control of distributed generators in the energy Internet," *IEEE Trans. Smart Grid*, vol. 6, no. 6, pp. 3006–3019, Nov. 2015.
[26] X. Zhou, M. Liu, Y. Ma, B. Yang, and F. Zhao, "Linear active disturbance rejection control for DC bus voltage of permanent magnet synchronous generator based on total disturbance differential," *Energies*, vol. 12, no. 20, p. 3906, Oct. 2019, doi: 10.3390/en12203906.
[27] A. A. Godbole, J. P. Kolhe, and S. E. Talole, "Performance analysis of generalized extended state observer in tackling sinusoidal disturbances," *IEEE Trans. Control Syst. Technol.*, vol. 21, no. 6, pp. 2212–2223, Nov. 2013.
[28] H. Jing-Qing, *Active Disturbance Rejection Control Technology-The Control Technology for Estimating and Compensating the Uncertainties*. Beijing, China: China Defensive Industry Press, 2008.
[29] D. Ma, X. Hu, H. Zhang, Q. Sun, and X. Xie, "A hierarchical event detection method based on spectral theory of multidimensional matrix for power system," *IEEE Trans. Syst., Man, Cybern. Syst.*, early access, Aug. 9, 2019, doi: 10.1109/TSMC.2019.2931316.
[30] L. Huang, H. Xin, Z. Li, P. Ju, H. Yuan, Z. Lan, and Z. Wang, "Grid-synchronization stability analysis and loop shaping for PLL-based power converters with different reactive power control," *IEEE Trans. Smart Grid*, vol. 11, no. 1, pp. 501–516, Jan. 2020.
[31] J. Ouyang, M. Li, Z. Zhang, and T. Tang, "Multi-timescale active and reactive power-coordinated control of large-scale wind integrated power system for severe wind speed fluctuation," *IEEE Access*, vol. 7, pp. 51201–51210, 2019.
[32] A. Krama, L. Zellouma, A. Benaissa, B. Rabhi, M. Bouzidi, and M. F. Benkhoris, "Design and experimental investigation of predictive direct power control of three-phase shunt active filter with space vector modulation using anti-windup PI controller optimized by PSO," *Arabian J. Sci. Eng.*, 44, pp. 6741–6755, Nov. 2019.
[33] X. N. Xu, X. S. Zhou, Y. J. Ma, and Z. Q. Gao, "Micro grid operation controller based on ADRC," *High Volt. Eng*, vol. 42, pp. 3336–3346, 2016.
[34] K. O. Oureilidis, E. A. Bakirtzis, and C. S. Demoullas, "Frequency-based control of island micro-grid with renewable energy sources and energy storage," *J. Mod. Power Syst. Clean Energy*, vol. 4, pp. 54–62, 2016.
[35] M. A. Hossain, H. R. Pota, A. M. O. Haruni, and M. J. Hossain, "DC-link voltage regulation of inverters to enhance microgrid stability during network contingencies," *Electr. Power Syst. Res.*, vol. 147, pp. 233–244, Jun. 2017.
[36] T. Yanghong, Z. Haixia, and Z. Ye, "A Simple-to-Implement fault diagnosis method for open switch fault in wind system PMSG drives without threshold setting," *Energies*, vol. 11, no. 10, p. 2571, Sep. 2018.
[37] S. Y. Hou, Y. Fang, and J. X. Zeng, "Application of supercapacitors to improve wind power system's low voltage ride through capability," *Electr. Mach. Control*, vol. 14, pp. 23–31, 2010.
[38] J. Ouyang, Z. Zhang, T. Tang, M. Pang, M. Li, and D. Zheng, "Fault overload control method for high-proportion wind power transmission systems based on emergency acceleration of doubly-fed induction generator," *IEEE Access*, vol. 7, pp. 32874–32883, 2019.
[39] C. Zhang, M. Molinas, A. Rygg, J. Lyu, and X. Cai, "Harmonic transfer-function-based impedance modeling of a three-phase VSC for asymmetric AC grid stability analysis," *IEEE Trans. Power Electron.*, vol. 34, no. 12, pp. 12552–12566, Dec. 2019.
[40] Z. Zhao, P. Yang, Y. Wang, Z. Xu, and J. M. Guerrero, "Dynamic characteristics analysis and stabilization of PV-based multiple microgrid clusters," *IEEE Trans. Smart Grid*, vol. 10, no. 1, pp. 805–818, Jan. 2019.

**YOUJIE MA** received the bachelor's, master's, and Ph.D. degrees in power system and automation from Tsinghua University, from 1982 to 1993, respectively. From 1993 to 2002, she worked with the School of Electrical and Automation Engineering, Qingdao University, where she was promoted to Full Professor, in 1998. Since 2002, she has been with the School of Automation, Tianjin University of Technology.

**LUYONG YANG** is currently pursuing the master's degree with the School of Electrical and Electronic Engineering, Tianjin University of technology, Tianjin, China.

His research interest includes the grid-connected control of new energy power generation systems.

**XUESONG ZHOU** received the bachelor's degree in electrical engineering from the South China University of Technology, Guangzhou, China, in 1984, and the master's and Ph.D. degrees in electrical engineering from Tsinghua University, in 1990 and 1993, respectively.

From 1993 to 2002, he was the Deputy Dean of the School of Electrical and Automation Engineering, Qingdao University. In 2002, he joined the Tianjin University of Technology as a Professor. His area of expertise is the development and use of power electronics and renewable energy.

**XIA YANG** was born in Hebei, China, in 1994. She is currently pursuing the master's degree with the School of Electrical and Electronic Engineering, Tianjin University of Technology, Tianjin, China.

Her research interests include the grid-connected control of wind power system and harmonics in new energy systems.